A Kinetic and Thermodynamic Framework for the Hammerhead Ribozyme Reaction†

Klemens J. Hertel,‡ Daniel Herschlag,*,§ and Olke C. Uhlenbeck*,‡

Department of Chemistry and Biochemistry, University of Colorado, Boulder, Colorado 80309-0215, and Department of Biochemistry, B400 Beckman Center, Stanford University, Stanford, California 94305-5307

Received October 11, 1993; Revised Manuscript Received December 27, 1993®

ABSTRACT: A hammerhead ribozyme (HH16) with eight potential base pairs in each of the substrate recognition helices stabilized product binding sufficiently to enable investigation of the ligation of oligonucleotides bound to the ribozyme. All individual rate constants for product association and dissociation were determined. The following conclusions were obtained for HH16 from the analysis performed at 50 mM Tris, pH 7.5, 10 mM $MgCl_2$, and 25 °C. (1) HH16 cleaves bound substrate with a rate constant of k_2 = 1 min^{-1}, similar to rate constants obtained with other hammerhead ribozymes. (2) k_{-2}, the rate of ligation of the 5′ product and 3′ product to form substrate, equaled 0.008 min^{-1}, indicating an approximately 100-fold preference for the formation of products on the ribozyme. This internal equilibrium, compared with that for the overall solution reaction, gives an effective concentration (EC) of 10^{-2} M for the two products bound to the ribozyme. This low EC suggests that upon cleavage of S the hammerhead complex acquires a "floppiness" which provides an entropic advantage for the formation of products on the ribozyme. (3) Product and substrate association rate constants were in the range of 10^7–10^8 M^{-1} min^{-1}, comparable to values determined for short helices. (4) The stabilities of ribozyme/product complexes were similar to affinities predicted from helix–coil transitions of simple RNA duplexes, providing no indication of additional tertiary interactions. The products, P1 and P2, stabilize one another 4-fold on the ribozyme. (5) The dissociation constant for the binding of the substrate to the ribozyme was estimated to be about 10^{-17} M. These results allowed the construction of a free energy profile for the reaction of HH16, and provide a basis for future mechanistic studies.

Several plant viroids and virusoids autolytically cleave at a specific phosphodiester bond (Buzayan et al., 1986a,b; Hutchins et al., 1986; Prody et al., 1986). A consensus secondary structure of approximately 55 nucleotides termed the "hammerhead" domain has been identified (Buzayan et al., 1986b; Forster & Symons, 1987a,b) which can be assembled from 2 or 3 separate RNA molecules. Thus, the self-cleaving reaction has been turned into a multiple turnover reaction, with separate oligonucleotides acting as the "ribozyme" and the "substrate" (Figure 1) (Sampson et al., 1987; Uhlenbeck, 1987; Haseloff & Gerlach, 1988; Koizumi et al., 1988, 1989; Jeffries & Symons, 1989).

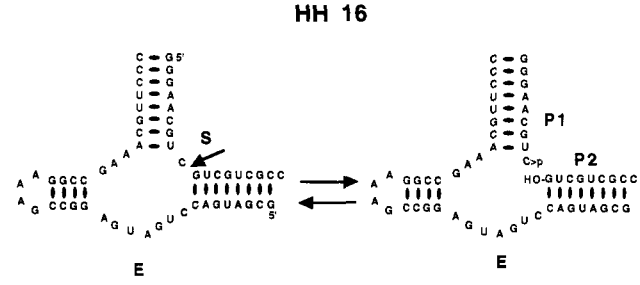

FIGURE 1: Secondary structure and reaction of hammerhead 16 (HH16). Using standardized hammerhead nomenclature (Hertel et al., 1992), the ribozyme (E), comprised of 38 nucleotides, catalyzes the cleavage of a specific phosphodiester bond within its 18-nucleotide-long substrate (S-C), generating two 9-nucleotide-long products. P2-C binds to E to form helix I; P1 binds to E to form helix III.

A minimal kinetic description for one turnover of the hammerhead ribozyme reaction (Figure 2) involves (1) assembly of ribozyme (E)[1] and substrate (S) into an E·S complex, (2) cleavage of the phosphodiester bond, generating a 5′ product with a 2′,3′-cyclic phosphate terminus (P1) and a 3′ product with a 5′-hydroxyl terminus (P2) that remain bound to the ribozyme, and (3) two pathways for release of the products. Each individual step is defined by elemental rate constants in the forward and reverse direction. A recent kinetic analysis of several different hammerhead sequences revealed that substrate length above 13 nucleotides and sequence had little effect on the rate constant of cleavage but that differences were observed for the substrate affinity to the ribozyme (Fedor & Uhlenbeck, 1992). However, the relatively low affinities of the products to the ribozymes used in that study prevented an analysis of the reverse reaction and the determination of individual product association and dissoci-

† This work was supported by NIH Grants GM 36944 and GM 37552 to O.C.U. and by a grant from the Lucille P. Markey Charitable Trust to D.H. D.H. is a Lucille P. Markey Scholar in Biomedical Science.

* Correspondence should be addressed to either one of these authors.

‡ University of Colorado.

§ Stanford University.

® Abstract published in *Advance ACS Abstracts,* February 15, 1994.

[1] Abbreviations: P1, GGGAACGUC>p; p^{32}P1, p^{32}GGGAACGUC>p; P1-G, GGGAACGUCG; P1-3′p, GGGAACGUC3′-p; P2, GUCGUCGC; P2-C, GUCGUCGCC; P2-p^{32}Cp, GUCGUCGCp^{32}Cp; S-C, GGGAACGUCGUCGUCGCC; p^{32}S-C, p^{32}GGGAACGUCGUCGUCGCC; S-p^{32}Cp, GGGAACGUCGUCGUCGCp^{32}Cp; S, GGGAACGUCGUCGUCGC; p^{32}S, p^{32}GGGAACGUCGUCGUCGC; E, ribozyme; HH16, hammerhead cleavage motif comprised of separate ribozyme and substrate oligonucleotides (Figure 1); K_{eq}^{int} = [E·P1·P2]/[ES]; K_{eq}^{ext}, = [P1][P2]/[S]; ΔG^{ES}, free energy change of substrate binding to the ribozyme; $\Delta G^{initiation}$, free energy change for helix initiation associated with forming the first base pair in an RNA duplex, 3.2 kcal/mol at 25 °C; Tris, tris(hydroxymethyl)aminomethane; EDTA, (ethylenedinitrilo)-tetraacetic acid; EC, effective concentration; STobRV(+), satellite RNA of tobacco ringspot virus; ASBV, avocado sunblotch viroid; vLTSV, virusoid of lucerne transient streak virus.

0006-2960/94/0433-3374$04.50/0

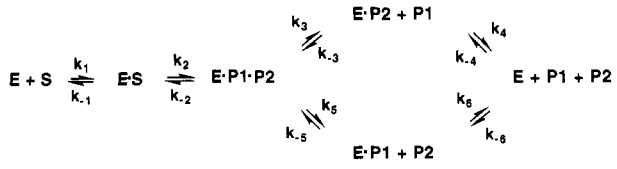

FIGURE 2: Minimal kinetic mechanism for intermolecular hammerhead catalysis.

ation rate constants. In contrast, other ribozymes such as the hairpin ribozyme or the group I intron from *Tetrahymena thermophilia* pre-rRNA have been observed to catalyze the reverse reaction (Buzayan et al., 1986a; Chowrira et al., 1993; Feldstein & Bruening, 1993; Woodson & Cech, 1989), and it was possible to determine product affinities for the *Tetrahymena* ribozyme (Herschlag & Cech, 1990; Pyle et al., 1990; Bevilacqua & Turner, 1991).

A new hammerhead ribozyme (HH16) was designed with eight potential base pairs in each of the substrate recognition helices (Figure 1). The helices of HH16 were designed to be stable enough to determine product binding and to investigate the reversal of the cleavage reaction, but not so stable as to prevent measurement of the multiple turnover rate. This has allowed us to determine elemental rate constants for the reverse reaction and rate and equilibrium constants for all steps of the hammerhead reaction outlined in Figure 2. The kinetic and thermodynamic analysis of HH16 reported here allows a better understanding of the binding and the catalytic behavior of the hammerhead ribozyme and provides a framework for mechanistic investigations and for the design of hammerhead ribozymes directed for gene inactivation (Uhlenbeck, 1993).

MATERIALS AND METHODS

RNA Synthesis and Characterization. The oligonucleotides E[1] and S were synthesized by *in vitro* transcription with T7 RNA polymerase using synthetic DNA templates (Milligan & Uhlenbeck, 1989). S, P2, and P1-G were synthesized chemically as previously described (Fedor & Uhlenbeck, 1992). All oligonucleotides were purified by electrophoresis using denaturing 20% polyacrylamide/7 M urea gels, ethanol-precipitated, and stored in 50 mM Tris-HCl (pH 7.5) at −20 °C (Fedor & Uhlenbeck, 1990). The rate and extent of reaction of chemically synthesized S were identical to those for S obtained by T7 transcription.

The 5′ cleavage product P1 which contains a 2′,3′-cyclic terminus was generated by periodate oxidation of P1-G followed by β-elimination to give P1 with a 3′-phosphate and then treatment with a water-soluble carbodiimide to form the cyclic phosphate (Naylor & Gilham, 1966). Specifically, a 50-μL reaction mixture containing 200 μM P1-G, 10 mM $NaIO_4$, and 50 mM sodium acetate, pH 6.5, was incubated for 15 min at 60 °C followed by the addition of 25 μL of 0.6 M lysine, pH 9. The solution was then left at room temperature for 45 min to generate P1-3′p. The 3′-phosphorylated product was purified by 20% denaturing gel electrophoresis. The 2′,3′-cyclic phosphate was generated by incubating purified P1-3′p with 50 mM 1-ethyl-3-[3-(dimethylamino)propyl]carbodiimide in 100 mM MES buffer, pH 5.5, for 1 h at 37 °C. P1 was then purified by 20% denaturing gel electrophoresis, which gave separation of the cyclic product from the 3′-phosphate starting material. The yield of the cyclization reaction was typically >90%.

5′-End-labeling of oligonucleotides synthesized by T7 RNA polymerase was accomplished by removing 5′-triphosphate with calf intestine alkaline phosphatase followed by reaction with [γ-^{32}P]ATP and T4 polynucleotide kinase. Chemically synthesized oligonucleotides were 5′-end-labeled directly with [γ-^{32}P]ATP. 3′-End-labeling of oligonucleotides was accomplished with [^{32}P]pCp and T4 RNA ligase (England & Uhlenbeck, 1978). To verify that the transcription products contained the correct 3′-end, isolated oligonucleotides were 3′-end-labeled with [^{32}P]pCp, digested with ribonuclease T_2, and analyzed by two-dimensional thin-layer chromatography (Kochino et al., 1980). Oligonucleotide concentrations were determined from specific activities for radioactive RNAs and assuming a residue extinction coefficient of 260 nm of 8.5 × 10^3 M^{-1} cm^{-1} for nonradioactive RNA.

Because of the requirement to 3′-end-label the 3′ cleavage product in order to maintain the 5′-hydroxyl terminus of P2, a dangling C residue was added to S to give the analogous oligonucleotide substrate, S-C (Figure 1). The oligonucleotides S and P2, lacking the terminal C, were 3′-end-labeled with [^{32}P]pCp to generate S-p^{32}Cp and P2-p^{32}Cp. 5′-End-labeling of oligonucleotides S and P1 generated p^{32}S and p^{32}-P1. Control experiments established that the lack of the terminal nucleotide in protocols where an excess of unlabeled S or P2 was used as chase molecule or nonradioactive ligand had no effect on the measured rate constants.

Nondenaturing gel electrophoresis was used to check for stable conformational forms that might affect the reaction kinetics. E, S, P1, and P2 were analyzed under cleavage conditions at concentrations ranging from 1 to 2000 nM, as previously described (Fedor & Uhlenbeck, 1990).

Individual Rate and Equilibrium Constants. All reactions reported here were conducted at 25 ± 0.5 °C in a buffer containing 50 mM Tris-HCl, pH 7.5, and 10 mM $MgCl_2$, as previously described (Fedor & Uhlenbeck, 1990, 1992). All frozen oligonucleotide solutions were heat-treated at 95 °C for 1.5 min in 50 mM Tris-HCl (pH 7.5 at 25 °C) in order to disrupt potential RNA aggregates formed during storage. The solutions were then allowed to equilibrate for 10 min at reaction temperature. To assay for cleavage, reaction samples were quenched with 3× volume of "denaturing quench buffer" (8 M urea, 50 mM EDTA, pH 8, 0.02% bromophenol blue, and 0.02% xylene cyanol) and separated on a denaturing 20% polyacrylamide/7 M urea gel. To assay for complex formation, samples were loaded onto a native 15% polyacrylamide gel immediately after adding 0.1 volume of "native gel loading buffer" (50% sucrose, 0.02% bromophenol blue, and 0.02% xylene cyanol). Radioactive bands were located and quantitated using a Molecular Dynamics radioanalytical scanner. Rate constants which describe the first-order disappearance of the signal were obtained from semilogarithmic plots according to the equation $\log [A] = (-k/2.303)t$. Since this equation is a linear algebraic expression, a plot of the log of the concentration of signal as a function of time yields a straight line. The slope of this line is equal to $-k/2.303$.

Each rate constant reported here is the average of at least three determinations. Unless stated explicitly, experiments conducted side-by-side display a high degree of precision (<10% variation), while the variation in rate constants was larger (usually <25%) when the experiments were performed on different days with different solutions. Equilibrium dissociation constants (K_d) are reported as an average of three independent binding curves. The standard deviation was less than 2-fold.

k_2. Single-turnover experiments with ribozyme in excess over substrate were used to determine the first-order rate constant for cleavage of p^{32}S (or p^{32}S-C) in the E·S complex. Each ribozyme and substrate solution was heat-treated separately, adjusted to the final concentration of 10 mM

$MgCl_2$, and then allowed to reach reaction temperature. Reactions were initiated by combining various concentrations of E (10–5000 nM) in 10 μL of reaction buffer with 10 μL of a 2 nM solution of $p^{32}S$ in reaction buffer. Aliquots (1.5 μL) were removed at appropriate intervals and quenched with 10 μL of denaturing quench buffer. Using this protocol, reactions were first order with end points of 70–75%.

To verify that saturation was obtained at the higher enzyme concentrations, a different reaction protocol was used in which E (550–2800 nM) and $p^{32}S$ (1 nM) were heat-treated together in 18 μL of 55 mM Tris-HCl (pH 7.5). After equilibration to 25 °C, the reaction was initiated by the addition of 2 μL of $MgCl_2$ to a final concentration of 10 mM. The amount of substrate cleaved using this protocol varied between 80% and 85%.

Rate constants for reaction were determined from the slope of semilogarithmic plots of the fraction of $p^{32}S$, normalized to the final extent of cleavage, versus time.

k_{-2}. To measure the reversal of the chemical step, k_{-2}, an 18-μL solution containing 1.1 nM P2-p^{32}Cp, 550 nM ribozyme, and 1100 nM unlabeled P1 was heat-treated at 95 °C for 1.5 min and allowed to reach reaction temperature, and the reaction was initiated by the addition of 2 μL of 100 mM $MgCl_2$. Samples were removed and quenched in denaturing quench buffer at times ranging from 15 s to 30 min. Observed reaction rate constants were obtained from the slopes of semilogarithmic plots of the fraction of P2-p^{32}Cp ligated, normalized to the final extent of the reaction, versus time. The value of k_{-2} was determined from the observed rate constant as described under Results.

k_3, k_4, k_5, and k_6. The dissociation rate constants of products P1 or P2-C in the presence of the other, k_3 and k_5, were measured by a pulse–chase protocol, followed by analysis of ribozyme/product complexes using native gel electrophoresis. In a typical experiment to measure k_3, 4 μL of 10 nM p^{32}P1, 500 nM E, and 1000 nM P2 in reaction buffer were incubated for 15 min at 25 °C to allow complete binding. A chase reaction was then initiated by the addition of 36 μL of 2.8 μM unlabeled P1 in reaction buffer to follow the practically irreversible dissociation of p^{32}P1. The final chase concentrations were 50 nM enzyme, 1 nM p^{32}P1, 2500 nM P1, and 100 nM P2 in 40 μL. Time points (3 μL) were taken, adjusted with 0.3 μL of native gel loading buffer, and immediately loaded onto a running 15% native polyacrylamide gel containing 10 mM $MgCl_2$/50 mM Tris–acetate, pH 7.5. Dissociation rates were obtained from the slopes of semilogarithmic plots of the fraction p^{32}P1 complexed to E·P2, normalized to the final extent of dissociation, versus time. The initial concentration of P2 of 1000 nM is well above its K_d of approximately 0.3 nM (see Results) so that dissociation of p^{32}P1 from the E·p^{32}P1·P2 complex was followed.

To verify the native gel determinations, the same experiment was analyzed by following the extent of product ligation by denaturing gel electrophoresis. For k_3, 4 μL of 10 nM p^{32}P1, 500 nM E, and 1000 nM P2 in reaction buffer were allowed to reach equilibrium for ligation (~15 min). To initiate the dissociation reaction, 36 μL of 2.8 μM nonradiolabeled P1 in cleavage buffer was added to 4 μL of the equilibrium mixture to give final concentrations of 50 nM ribozyme, 1 nM p^{32}P1, 100 nM P2, and 2500 nM P1. The decrease in $p^{32}S$ concentration was followed over time to obtain the dissociation rate constant for p^{32}P1. The dissociation rate constant was computed from a semilogarithic plot of the data, normalized to the final extent of $p^{32}S$.

The same experiments were conducted at identical concentrations to measure k_5 except that P2-p^{32}Cp was used as a marker in the presence of E and P1 and an excess of P2 was used in the chase reaction.

The dissociation rate constants of products P1 and P2-C in the absence of the other, k_4 and k_6, were measured by the native gel pulse–chase protocol described above. In a typical experiment to measure k_6, 4 μL of 10 nM p^{32}P1 and 500 nM E in reaction buffer were incubated for 15 min at 25 °C to allow complete binding. The chase reaction was initiated by the addition of 36 μL of 2.8 μM nonradiolabeled P1 in reaction buffer. The final chase concentrations were 50 nM enzyme, 1 nM p^{32}P1, and 2500 nM P1 in 40 μL. Reaction rates were obtained from the slopes of semilogarithmic plots of the fraction of p^{32}P1 complexed to E, normalized to the final extent of dissociation, versus time.

k_{-3}, k_{-4}, k_{-5}, and k_{-6}. The individual product association rates, k_{-3}, k_{-4}, k_{-5}, and k_{-6}, were measured by "pulse quench native gel electrophoresis". Typically, as for the k_{-5} determination, 2 μL of a 5 nM P2-p^{32}Cp solution in reaction buffer was combined with 18 μL of a 5–30 nM ribozyme solution containing 100 nM P1 in reaction buffer. Aliquots (2 μL) were removed at intervals, and additional binding was quenched with 0.5 μL of native gel loading buffer that contained 500 nM unlabeled P2. Each time point was immediately loaded onto a running 15% nondenaturing polyacrylamide gel containing 10 mM $MgCl_2$/50 mM Tris–acetate, pH 7.5, at 4 °C. Since the binding quench step is equivalent to the dissociation chase described above, 100% complex formation was never observed. Analysis of the data therefore required normalization to the final extent of binding for each experiment. k_{-3}, k_{-4}, and k_{-6} were measured by the same protocol except p^{32}P1 was used as radiolabel and/or the other product was omitted.

k_{-1}. The upper limit of the substrate dissociation rate constant, k_{-1}, was determined by pulse–chase experiments (Herschlag & Cech, 1990; Fedor & Uhlenbeck, 1992). Typically, 3 μL of 1 nM $p^{32}S$ (or p^{32}S-C) in reaction buffer was combined with 9 μL of 670 nM E in reaction buffer. After an initial binding period of t_1 = 30 s, 18 μL of 8.3 μM nonradiolabeled substrate S was added, initiating the chase. The time of 30 s for t_1 allows essentially complete formation of the E·$p^{32}S$ complex as it is 5–10-fold greater than the half-time for binding under these conditions ($k_{obs} = k_1[E]$). During the chase period, t_2, aliquots were removed and quenched in denaturing quench buffer. In a control reaction which was conducted at the same time, 5 μL of $p^{32}S$ (1 nM) was allowed to react with 15 μL of 670 nM E. Observed reaction rates were obtained from slopes of semilogarithmic plots of the amount of substrate, normalized to the final extent of reaction, versus time. No significant cleavage of $p^{32}S$ was observed in experiments in which $p^{32}S$ was combined with nonradiolabeled S prior to the addition of ribozyme, indicating that the chase conditions used did not allow rebinding of $p^{32}S$.

Modifications of the above protocol were used to evaluate the effect of the chase oligonucleotide and the extent of initial binding on the experiment. For example, 1 μL of 1 nM $p^{32}S$ in reaction buffer was combined with 3 μL of 670 nM E in reaction buffer. After an initial binding period of 30 s, t_1, 4000 μL of reaction buffer instead of an excess of oligonucleotide was added to initiate a "dilution" chase. Aliquots (40 μL) were removed, and analyzed as described above. The dilution chase was shown to be effective in preventing rebinding of $p^{32}S$ by monitoring cleavage when 1 μL of $p^{32}S$ and 4000 μL of dilution buffer were combined prior to the addition of

3 μL of 670 nM E. No significant cleavage of $p^{32}S$ was observed over the time of the pulse–chase experiment. In another reaction protocol, E (670 nM) and $p^{32}S$ (1.1 nM) were heat-treated together in 10.8 μL of 55 mM Tris-HCl (pH 7.5) to preanneal E and $p^{32}S$. After equilibration to 25 °C, an oligonucleotide chase reaction was initiated by the addition of 19.2 μL of 7.8 μM nonradiolabeled S in 16.6 mM $MgCl_2$ to give a final concentration of 10 mM $MgCl_2$.

k_1. The rate constant for substrate binding, k_1, was measured using a series of pulse–chase experiments. Several concentrations of ribozyme ranging from 5 to 120 nM in reaction buffer were combined with 1 nM $p^{32}S$ in reaction buffer according to the protocol described above for measuring k_{-1}. For each ribozyme concentration, several chase reactions were initiated at various times, t_1 ranging from 15 to 120 s, effectively quenching the binding of $p^{32}S$ to E. At t_2 = 15 min, greater than 6 times the $t_{1/2}$ for the cleavage reaction, the amount of product was measured. Under these conditions, $k_{obs} = k_{on}[S] + k_{off}$ [as described in Herschlag and Cech (1990)].

K_d of Ribozyme/Product Complexes. Equilibrium dissociation constants (K_d) of each product/ribozyme complex were measured using nondenaturing gel electrophoresis (Pyle et al., 1990). Thirteen ribozyme concentrations ranging from 0.01 to 200 nM and 0.002 nM $p^{32}P1$ or P2-$p^{32}Cp$ in 50 μL of reaction buffer were allowed to reach equilibrium at 25 °C for 20–96 h. Each 50-μL sample was adjusted with 2 μL of native gel loading buffer prior to loading onto a 15% polyacrylamide native gel. To correct for the fraction of ligand which was unable to bind the ribozyme or which dissociated while entering the gel, each sample was normalized to the maximal extent of complex observed. K_d values were then obtained from a nonlinear least-squares fit (KaleidaGraph, Ablebeck Software).

RESULTS

Testing the Oligonucleotides for Conformational Heterogeneity. Before the detailed kinetic investigation of the hammerhead reaction was initiated, the oligonucleotides $p^{32}E$, $p^{32}S$, $p^{32}P1$, and P2-$p^{32}Cp$ were tested for alternate conformations that might affect the kinetic analysis. Each RNA was subjected to nondenaturing gel electrophoresis at cleavage conditions (Fedor & Uhlenbeck, 1990) at concentrations ranging from 1 to 2000 nM. $p^{32}E$ migrates as a single species over the tested range and was considered to be structurally homogeneous. $p^{32}S$ was observed to form a concentration-dependent alternate structure with an apparent equilibrium dissociation constant of 200 nM as judged by a shift in mobility to a slower migrating species with increasing concentration (data not shown). The complex exchanged rapidly to monomers upon dilution. On the basis of this information, experiments with $p^{32}S$ were conducted at concentrations much less than 200 nM, except when S was used as a chase molecule. While $p^{32}P1$ is homogeneous over the tested range, P2-$p^{32}Cp$ migrates as a doublet even at the lowest concentrations. This suggests that P2-$p^{32}Cp$ has two alternate intramolecular conformations. Analysis of the data using P2-$p^{32}Cp$ as a label required an additional normalization which is described below. These preliminary experiments defined the ranges of oligonucleotide concentrations used in the kinetic analysis. All elemental rate constants for the intermolecular hammerhead cleavage reaction, defined in Figure 2, were determined by kinetic and thermodynamic measurements. Several parameters were determined by independent methods, supporting the validity of the techniques used herein. Details of the procedure are outlined under Materials and Methods. The results of this analysis are described below and are summarized in Figure 10.

Determination of the Rate Constant for Cleavage, k_2. Experiments in which ribozyme was in excess over substrate were used to determine the first-order rate constant for cleavage of S in the E·S complex, k_2. When E and $p^{32}S$ were combined to initiate the reaction, the rates of cleavage observed at the lower ribozyme concentrations (5–40 nM) increased linearly with ribozyme concentration. At higher ribozyme concentrations (500–2500 nM), the observed rate of cleavage, k_{obs} = 0.8–1 min^{-1}, was independent of the ribozyme concentration, indicating that saturation of the substrate has been reached. Since an excess of E was used, the observed rate of cleavage is independent of product release and reflects the rate constant of cleavage, k_2, at saturating ribozyme conditions.

To support the interpretation that saturation of $p^{32}S$ accounts for the observed plateau, a different reaction protocol was used in which high concentrations of E (500–2500 nM) were preincubated with trace $p^{32}S$ in the absence of $MgCl_2$ to allow annealing to occur. Then $MgCl_2$ was added to initiate the reaction. Although the extent of the reaction was usually 10% higher, the observed rate constant of cleavage determined with this protocol were also 0.8–1 min^{-1} (data not shown). The value of k_2 = 1 min^{-1} is similar to values determined previously for other hammerhead constructs under similar conditions (Uhlenbeck, 1987; Ruffner et al., 1989; Fedor & Uhlenbeck, 1990, 1992; Dahm & Uhlenbeck, 1991; Perreault et al., 1991; Pieken et al., 1991).

The identical rate of cleavage of the E·S complex whether formed in the presence of $MgCl_2$ or preannealed in reactions initiated with the addition of $MgCl_2$ indicates that magnesium can bind after S and that magnesium binding must be at least 1 order of magnitude faster than the rate constant of cleavage, k_2 = 1 min^{-1}.

Rate Constant for Ligation, k_{-2}. Experiments monitoring the ligation of P1 and P2 in the E·P1·P2 complex to form the E·S complex were carried out to determine the rate of reversal of the chemical step, k_{-2}. At saturating concentrations of ribozyme, a small excess of P1, and a trace of P2-$p^{32}Cp$, ligation was measured by formation of small but readily detectable amounts of substrate (Figure 3A). As expected, the presence of both ribozyme and Mg^{2+} was required for ligation. The reaction reached an equilibrium of ~0.0065, and the value of k_{obs} = 0.95 min^{-1} (Figure 3B) is consistent with an approach to equilibrium involving a single step ($k_{obs} = k_2 + k_{-2}$). The extent and rate of reaction did not change in control experiments in which the concentrations of ribozyme (250–2000 nM) and P1 (500–4000 nM) were varied. This indicates that saturation had been achieved. Reactions of trace $p^{32}P1$ with saturating unlabeled P2 and ribozyme gave, within error, the same extent and rate of reaction.

The average fraction of S generated using either $p^{32}P1$ or P2-$p^{32}Cp$ as the radioactive marker was determined from several experiments to be 0.0075 ± 0.002. Thus, the internal equilibrium constant, K_{eq}^{int} = [E·P1·P2]/[E·S], is 130 (=1/0.0075). The values of K_{eq}^{int} = 130, the equation $K_{eq}^{int} = k_2/k_{-2}$, and k_2 = 1 min^{-1} give the rate constant for ligation of k_{-2} = 0.008 ± 0.003 min^{-1}. The rate of cleavage is much faster than the rate of ligation, resulting in a strong preference for the formation of products of the ribozyme.

Product Dissociation Rate Constants, k_3, k_4, k_5, k_6. Dissociation rate constants for each product with the other product bound (k_3 and k_5) were determined by pulse–chase native gel electrophoresis. The protocol for determining k_3

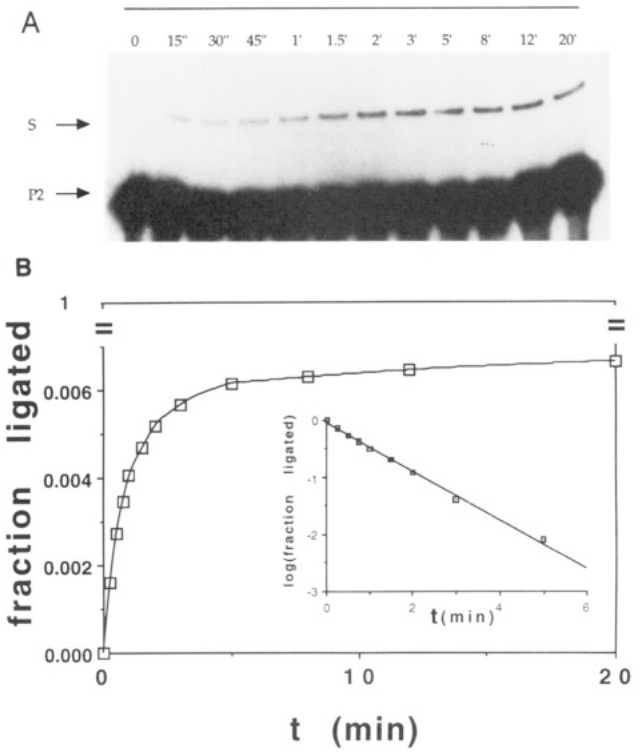

FIGURE 3: Rate and extent of ligation, k_{-2} and K_{eq}^{int}. (A) Autoradiogram of the ligation reaction in which $p^{32}S$ was formed in a reaction with 500 nM E, 1000 nM P1, and 1 nM P2-$p^{32}C$. (B) Quantitation of $p^{32}S$ formed with time for the autoradiogram in (A). The fraction of substrate formed approaches an equilibrium of $K_{eq}^{int} = k_2/k_{-2} \sim 0.0065$. A semilogarithmic plot (inset) of the normalized data in (B) gives the value of k_{obs} ($=k_2 + k_{-2}$) = 0.95 min^{-1} for the ligation reaction.

Scheme 1

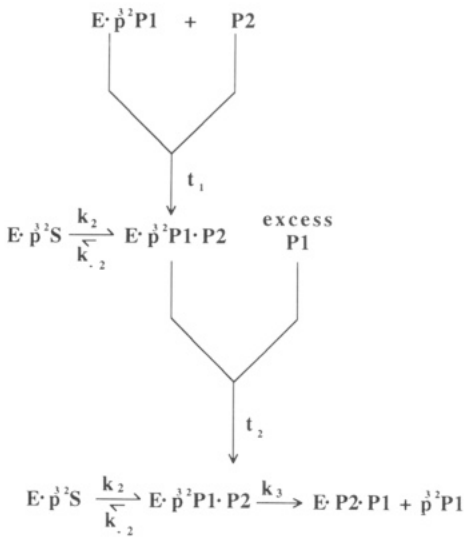

is shown in Scheme 1. At saturating ribozyme concentrations, a small excess of P2 and a trace concentration of $p^{32}P1$ were combined. After sufficient time was allowed for E·p^{32}P1·P2 formation (period t_1), an excess of unlabeled P1 was added. The high concentration of chase molecule relative to ribozyme and $p^{32}P1$ ensured that essentially every labeled product molecule that dissociated from the ribozyme during the chase was replaced by an unlabeled P1. The decrease in E·p^{32}P1·P2 ternary complex observed on native gels as a function of time t_2 is shown in Figure 4A. The rate constant of $k_3 = 0.04$ min^{-1} was obtained from the slope in Figure 4C.

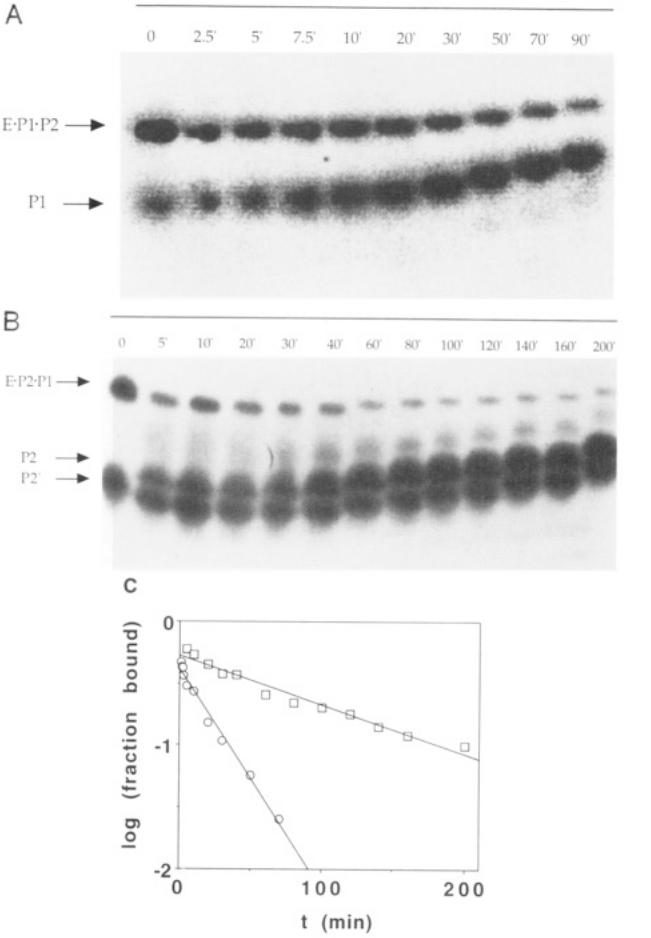

FIGURE 4: Pulse–chase native gel electrophoresis measuring the rate constants for product dissociation, k_3 and k_5. (A) Phosphoimager printout of a polyacrylamide gel showing the time-dependent dissociation of $p^{32}P1$ from the E·p^{32}P1·P2 complex during a chase reaction with 50 nM E, 1 nM $p^{32}P1$, 100 nM P2, and 2500 nM unlabeled P1. (B) Autoradiogram of a polyacrylamide gel showing the time-dependent dissociation of P2-$p^{32}C$ from the E·P1·P2-$p^{32}C$ complex during a chase reaction with 50 nM E, 1 nM P2-$p^{32}C$, 1200 nM P1, and 2500 nM unlabeled P2. (C) Semilogarithmic plot for the dissociation of $p^{32}P1$ from E·p^{32}P1·P2 (○) from (A) and for the dissociation of P2-$p^{32}C$ from E·P1·P2-$p^{32}C$ (□) from (B). The slopes give $k_3 = 0.04$ min^{-1} and $k_5 = 0.009$ min^{-1}, respectively.

To measure k_5, a protocol analogous to Scheme 1 was used except that an excess of P1 and a trace of P2-$p^{32}Cp$ were used in the initial equilibrium and P2 was used to chase. As mentioned above, free P2-$p^{32}Cp$ exists in two conformers. As shown in Figure 4B (time 0 lane) and Figure 4C, the initial extent of P2 complexed with E is only about 60%. During the time course of the chase reaction (lanes 5′–200′), free P2-$p^{32}Cp$ of a different mobility is generated upon dissociation from the E·P1·P2 complex (Figure 4B, P2). The intensity of the lower migrating P2-$p^{32}Cp$ band (Figure 4B, P2′) did not change significantly throughout the reaction. This suggests that one of the two conformers P2′ binds the ribozyme weakly or not at all. Analysis of the data therefore ignored this "inactive" fraction since it is not in equilibrium on the time scale of the experiment. The rate constant of $k_5 = 0.009$ min^{-1} was obtained from the slope in Figure 4C.

Several control experiments were carried out to examine if formation of the E·P1·P2 ternary complex was complete prior to reaction initiation. The length of preincubation, t_1, was varied between 10 and 30 min, and the concentrations of ribozyme (100–2500 nM) and P2 for k_3 or of P1 for k_5 (200–5000 nM) in the preincubation were also varied. None of these changes in conditions had significant effects in the extent

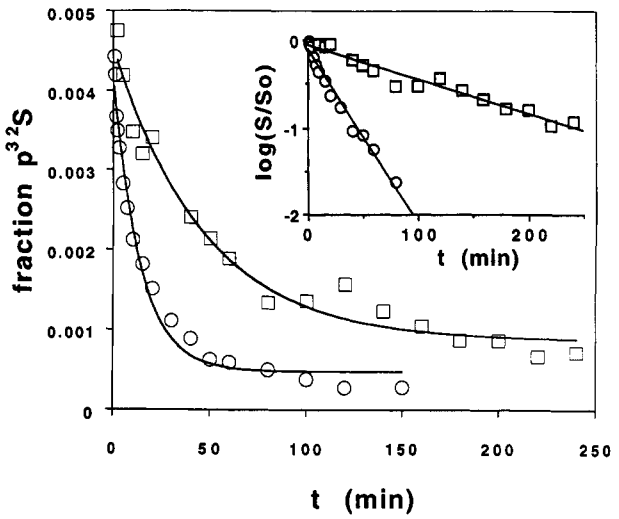

FIGURE 5: Product dissociation rate constants, k_3 (○) and k_5 (□), measured by ligation chase experiments. To measure k_3, (○), a solution of 1 nM p^{32}P1, 500 nM E, and 1000 nM P2 was allowed to reach equilibrium and was then challenged by a chase of unlabeled P1 to give final concentrations of 50 nM E, trace p^{32}P1 (1 nM), 100 nM P2, and 2500 nM unlabeled P1. The amount of p^{32}S present was followed as a function of time after challenge with unlabeled P1. To measure k_5, (□), the above protocol was followed except that P2 was labeled instead of P1 in the ligation chase of E·P1·P2-p^{32}C and 2500 nM unlabeled P2 was added instead of unlabeled P1. The slopes of a semilogarithmic plot for the disappearance of p^{32}S (inset) give the rate constants k_3 = 0.04 min^{-1} for the dissociation of p^{32}P1 from E·p^{32}P1·P2′ (○) and k_5 = 0.009 min^{-1} for the dissociation of P2-p^{32}C from E·P1·P2-p^{32}C (□). S/S_0 is the fraction of p^{32}S present at each time relative to that at t = 0.

Table 1: Summary of Product and Substrate Binding Affinities

complex	$K_{d,measured}$ (nM)[a]	$K_{d,calculated}$ (nM)[b]	k_{off} (min^{-1})[c]	$k_{on} \times 10^7$ (M^{-1} min^{-1})[d]
E·P2·p^{32}P1 ⇌ E·P2 + p^{32}P1	0.29	0.31	0.04	13
E·p^{32}P1 ⇌ E + p^{32}P1	1	1.7	0.1	5.8
E·P1·P2-p^{32}C ⇌ E·P1 + P2-p^{32}C	0.05	0.07	0.008	11
E·P2-p^{32}C ⇌ E + P2-p^{32}C	0.26	0.36	0.02	5.6
E·p^{32}S ⇌ E + p^{32}S	ND	4×10^{-9} [e]	7×10^{-11} [e]	1.8

[a] Measured by equilibrium native gel electrophoresis. [b] Calculated from k_{on} and k_{off}. [c] Product dissociation rate constants determined as outlined in Scheme 1. [d] Association rate constants determined by pulse–chase experiments (Schemes 2 and 3). [e] Estimated value based on K_{eq}^{int} and K_{eq}^{ext} as described under Discussion.

of initial complex formation or on the observed rate constants, indicating that binding was complete.

A ligation chase experiment was performed to provide a distinct method to measure k_3 and k_5. In this experiment, the same protocol was used as outlined in Scheme 1, but product dissociation was followed by the decrease in the amount of substrate as a function of t_2 by analysis on denaturing gels. The relative amount of p^{32}S (or S-p^{32}Cp), generated by ligation of p^{32}P1 and P2 (or P2-p^{32}Cp and P1), depends on the amount of labeled product complexed to E. Since the cleavage/ligation equilibrium proceeds much more rapidly than product dissociation, the decrease in p^{32}S (or S-p^{32}Cp) during the chase directly reflects the dissociation of p^{32}P1 (or P2-p^{32}Cp) from the ribozyme. The values of product dissociation obtained from these experiments, k_3 = 0.04 min^{-1} and k_5 = 0.008 min^{-1} (Figure 5), are in excellent agreement with those values determined by native gel electrophoresis of k_3 = 0.04 min^{-1} and k_5 = 0.009 min^{-1} (Figure 4). These results indicate that

Scheme 2

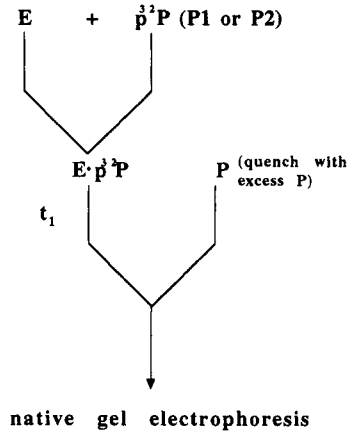

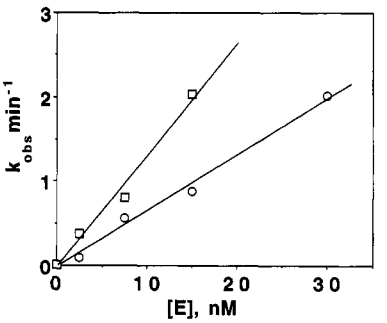

FIGURE 6: Product association rate constants determined by pulse–quench native gel electrophoresis. Since $k_{obs} = k_{on}[E] + k_{off}$, the slope of the plot of k_{obs} versus [E] gives the rate constant of product association. The observed constant for binding at each [E] was obtained from semilogarithmic plots of the fraction of complex formed versus time (data not shown). The points at [E] = 0 are from independent product dissociation pulse–chase experiments described in the text. The slope of the lines gives $k_{-4} = 5.6 \times 10^7$ M^{-1} min^{-1} for P2-p^{32}C binding to E (○) and $k_{-5} = 1.1 \times 10^8$ M^{-1} min^{-1} for P2-p^{32}C binding to E·P1 (□).

native gel electrophoresis can reliably measure relatively slow dissociation rate constants.

The dissociation rate constants for each product in the absence of the other (k_4 and k_6) were determined by pulse–chase native gel electrophoresis analogous to Scheme 1 but with the other product omitted. All of the product dissociation rate constants are given in Table 1. A comparison of the data indicates that P1 bound to the ribozyme slows the rate of dissociation of P2 about 2-fold and vice versa.

Product Association Rate Constants, k_{-3}, k_{-4}, k_{-5}, k_{-6}. All product association rate constants were determined as outlined in Scheme 2. A trace amount of labeled product was allowed for varying times t_1 to complex with ribozyme, either in the presence or in the absence of the other product. Further binding was quenched by adding excess unlabeled product, and the amount of complex formed at each time t_1 was analyzed by native gel electrophoresis. At each ribozyme concentration, an observed rate constant for binding was obtained ($k_{obs} = k_{on}[E] + k_{off}$), and the slope of a plot of these observed rate constants against ribozyme concentration gave the second-order rate constant for P2-C binding to E of $k_{-4} = 5.6 \times 10^7$ M^{-1} min^{-1} and P2-C binding to the E·P1 complex of $k_{-5} = 1.1 \times 10^8$ M^{-1} min^{-1} (Figure 6). All product association rate constants are summarized in Table 1. The data indicate that bound P1 increases the association rate constant of P2 about 2-fold and vice versa.

Equilibrium Dissociation Constants for Ribozyme/Product (E·P) Complexes. Equilibrium dissociation constants, K_d,

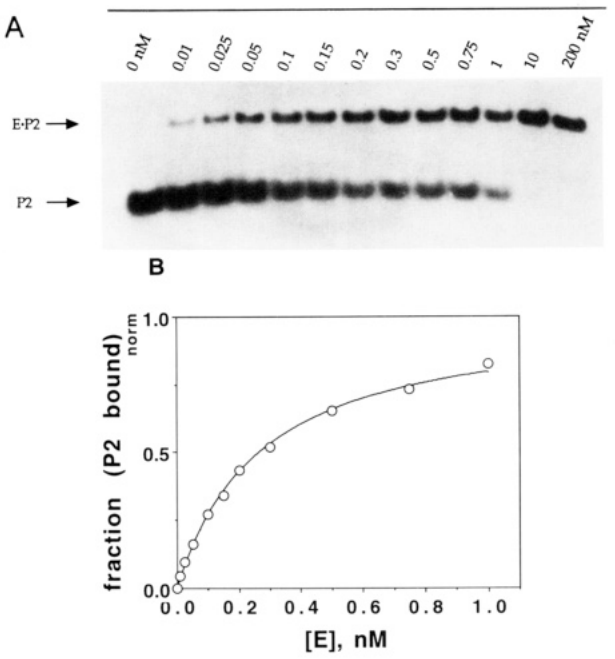

FIGURE 7: Equilibrium native gel electrophoresis of the E·P2-p^{32}C complex. (A) Autoradiogram of P2-p^{32}C binding to various concentrations of E after a 24-h incubation at 25 °C. (B) Fraction of P2-p^{32}C complexed to E as a function of ribozyme concentration. Each data point was normalized to the maximal extent of complexation, which was about 0.8 in a typical experiment. The line represents a nonlinear least-squares fit to the data and gives a dissociation constant K_d = [E][P2]/[E·P2] = 0.26 ± 0.05 nM.

can be calculated for each E·P complex from rate constants for association and dissociation ($K_{d,calculated} = k_{off}/k_{on}$, Table 1). In order to substantiate these calculations, K_d values were determined directly by equilibrium native gel electrophoresis. A typical binding profile is shown in Figure 7 for the binding of P2-p^{32}Cp to E. The results of all equilibrium dissociation determinations are summarized in Table 1. K_d values measured at the longest incubation time of 96 h did not differ significantly from K_d values determined after a 20-h incubation, ensuring that equilibrium had been reached prior to loading. The directly determined equilibrium dissociation constants are in excellent agreement with calculated values from the rate measurements (Table 1). The presence of P1 increases the affinity of P2 to the enzyme 4–5-fold and vice versa. These results support the validity of the individually measured product association and dissociation rate constants.

Rate of Substrate Dissociation, k_{-1}. Pulse–chase experiments were used to obtain an upper limit for the rate of substrate dissociation. As outlined in Scheme 3, substrate in the E·p^{32}S complex can partition between product formation (p^{32}P1 and P2, k_2) and dissociation, k_{-1}. Dissociation is irreversible in this experiment because of the high concentration of unlabeled S relative to ribozyme present during the chase period, t_2. The fraction p^{32}S cleaved to products during the chase period was identical to that observed in the reaction without chase (Figure 8), indicating that the rate constant for cleavage, k_2, is much faster than the dissociation rate constant of S, k_{-1}. Assuming an experimental uncertainty of 10%, this suggests that the rate of substrate dissociation, k_{-1}, is at least 10-fold slower than the rate of the chemical step, k_2.

The chase experiment was also conducted using modified protocols in which E and S were incubated together prior to magnesium addition. Additionally, rebinding of p^{32}S was prevented by a chase with unlabeled P2 instead of S or by using a 1000-fold "dilution chase" in order to determine

Scheme 3

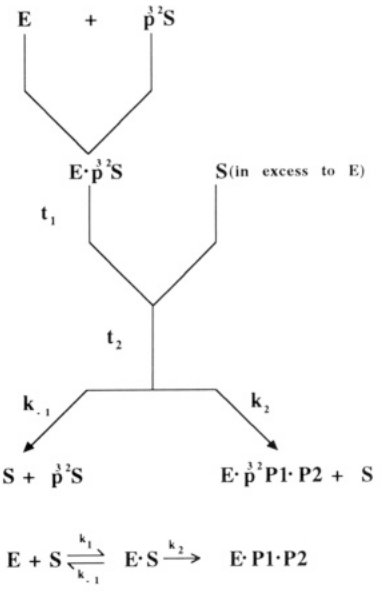

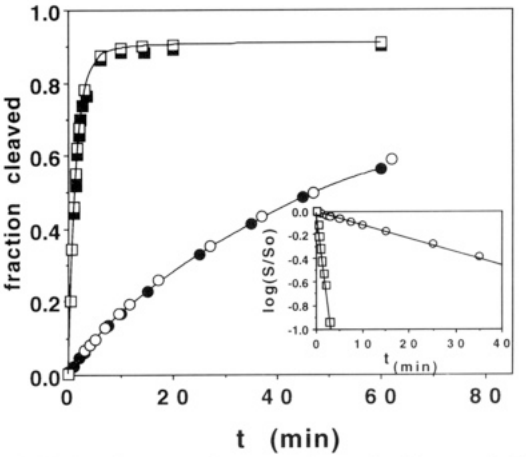

FIGURE 8: Pulse–chase experiments to determine the rate of substrate dissociation, k_{-1}. The fraction of substrate converted to products is shown for a reaction of 500 nM E combined with 1 nM p^{32}S. Either the reaction was diluted into 20 μM nonradioalabeled S chase [closed symbols, t_1 = 40 s (■, pH 7.5) or t_1 = 120 s (●, pH 6.5)], or the reaction was allowed to proceed without chase [open symbols, (□) pH 7.5; (○) pH 6.5]. A normalized semilogarithmic plot of the data (inset) gives k_2 values for the reaction without chase of 0.7 min^{-1} at pH 7.5 (□) and 0.03 min^{-1} at pH 6.5 (○).

whether the oligonucleotide used in the chase experiment affected the measured rate constant. All control reactions gave the same result described above, supporting the conclusion that the rate constant for cleavage, k_2, is much faster than k_{-1}, the dissociation rate constant of S.

An attempt was made to obtain detectable dissociation of substrate by decreasing the rate of the chemical step. Lowering the pH from 7.5 (Tris) to 6.5 (Pipes) slows k_2 about 10-fold (Dahm et al., 1993), allowing the substrate more time to dissociate. Even during the pH 6.5 chase, the same amount of p^{32}S was converted to products as in the control reaction (Figure 8). Dissociation of p^{32}S is therefore at least 1 order of magnitude slower than the observed rate of cleavage at pH 6.5, k_2 = 0.03 min^{-1}. This sets an upper limit for the rate of substrate dissociation of $k_{-1} < 0.003$ min^{-1}. Thus, essentially every time the E·p^{32}S is formed it goes on to form products. Experiments using p^{32}S-C as the radioactive substrate gave identical results.

Rate of Substrate Association, k_1. As described above, the rates of substrate cleavage increased linearly at the lower,

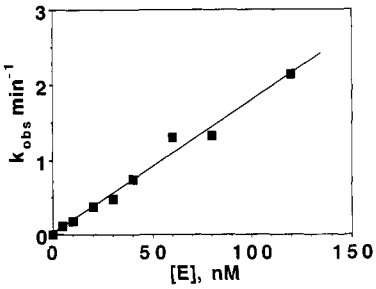

FIGURE 9: Rate of substrate binding, k_1. The value of k_{obs}, which is equal to $k_{obs} = k_1[E] + k_{-1}$, was measured in a series of pulse–chase experiments with varying ribozyme concentrations (data not shown). The slope of the plot of ribozyme concentration versus k_{obs} gives the rate constant for substrate binding, $k_1 = 1.8 \times 10^7$ M^{-1} min^{-1}. The y-intercept at [E] = 0 represents an estimate of the maximum substrate dissociation rate constant, $k_{-1} = 0.003$ min^{-1}, obtained from Figure 8 as described in the text.

subsaturating ribozyme concentrations ([E] = 5–40 nM). This linear increase reflects the second-order rate constant, k_{cat}/K_m, for the reaction of free E and free S, a measure which describes how efficiently free ribozyme reacts with free S. The experimental value for the observed second-order rate constant k_{cat}/K_m was 1.5×10^7 M^{-1} min^{-1} (data not shown). Since k_2 is much larger than k_{-1}, the observed second-order rate constant $k_{cat}/K_m = k_2k_1/(k_2 + k_1)$ reduces to k_1. Thus, k_{cat}/K_m is predicted to be a direct measure of the substrate association rate constant, k_1.

To test this, the rate constant for association of S with E was measured directly using the pulse–chase method outlined in Scheme 3. Ribozyme and p^{32}S were combined for varying times, t_1, followed by addition of excess unlabeled p^{32}S to prevent further binding. Following addition of the chase, the mixture was left for a time $t_2 = 15$ min to ensure that essentially every p^{32}S that had complexed to E during time t_1 was converted to product. The amount of product formed as a function of time t_1, k_{obs}, describes the rate of approach to equilibrium (E + p^{32}S $\rightleftharpoons$ E·p^{32}S) and is the sum of the rate constants of the forward and the reverse reaction, $k_{obs} = k_1[E] + k_{-1}$. The slope of the plot k_{obs} vs [E] gives the rate constant of substrate association, $k_1 = 1.8 \times 10^7$ M^{-1} min^{-1} (Figure 9). This value is in good agreement with the apparent second-order rate constant $k_{cat}/K_m = k_1 = 1.5 \times 10^7$ M^{-1} min^{-1}. The y-intercept in Figure 9 is zero, within error, consistent with the above conclusion that substrate dissociation (k_{-1}) is very slow.

Comparison of Observed Steady-State Reaction Parameters with Those Predicted from Pre-Steady-State Determinations. One test of a kinetic scheme is whether or not it can account for the observed steady-state reaction. The scheme in Figure 10 meets this test. As suggested from the elemental rate constants, product release was observed to be rate-limiting in these multiple turnover reactions. In multiple turnover reactions, there is a burst of product formation that is stoichiometric with ribozyme, followed by slower subsequent turnover (data not shown). This is consistent with Figure 10 in which the chemical cleavage step (k_2) is faster than the product dissociation steps. The observed rate constant of approximately 1 min^{-1} for the burst phase is also in agreement with the rate constant determined for k_2.

The maximal rate constant of cleavage for HH16 at steady-state conditions under multiple turnover conditions with saturating amounts of substrate is $k_{cat} = 0.01$ min^{-1} (data not shown). This observed value of the maximal rate of cleavage was then compared to a calculated value using a partition analysis (Cleland, 1975). This method computes the net rate constant for branched pathways such as the one proposed for the hammerhead ribozyme reaction. Using the rate parameters summarized in Figure 10, the partition analysis[2] predicts that approximately 80% of the flux will release P1 first, and 20% of the flux will release P2 first with a maximal multiple turnover rate constant of $k_{cat} = 0.015$ min^{-1}. This is the same, within error, as the observed value of $k_{cat} = 0.01$ min^{-1}.

It is important to realize that this agreement does not prove that no other species or steps are involved in the steady-state reaction. For example, native gel experiments suggest that a molecule of S can bind to E·P2 or E·P1 to form ternary E·P2·S and E·P1·S complexes (data not shown). While it is conceivable that S could accelerate dissociation of P1 or P2 in the ternary complex via a branch migration mechanism, the agreement between the observed and predicted k_{cat} values gives no indication of a large contribution from such a process. However, given that the ternary complex can form, it does seem reasonable that, with saturating S, most of the reaction flux will proceed via the ternary ribozyme/product/substrate complexes. The analogous behavior has been observed for dihydrofolate reductase, for which a new NADPH substrate binds prior to the release of the tetrahydrofolate product (Fierke et al., 1987). In the dihydrofolate reductase reaction, NADPH enhances the dissociation of terahydrofolate by approximately 10-fold.

DISCUSSION

Isolation of individual reaction steps has allowed the determination of 11 of the 12 elemental rate constants of Figure 2. Most of these have been confirmed by a second

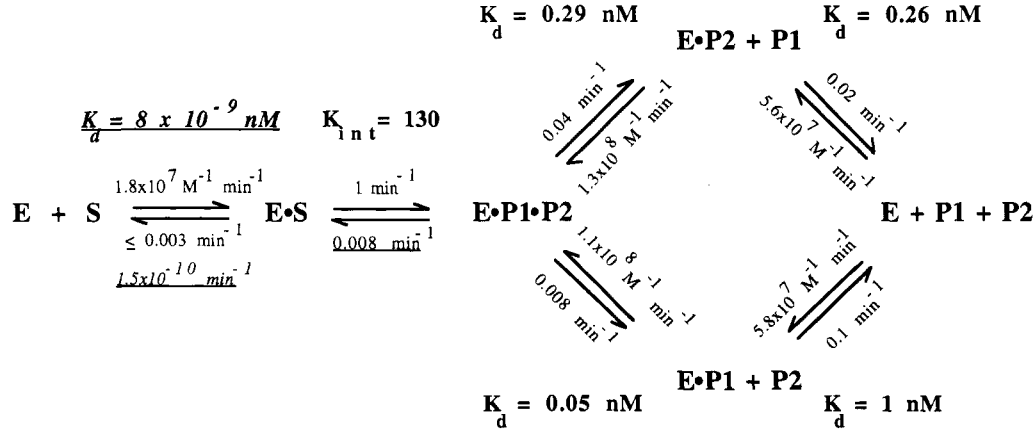

FIGURE 10: Summary of all determined rate constants defined in Figure 2. All underlined values were obtained by calculations (see text).

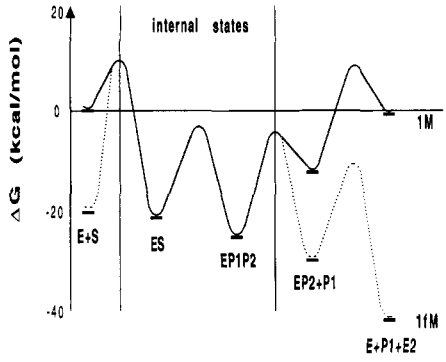

FIGURE 11: Free energy reaction profile for RNA cleavage by the hammerhead ribozyme. Only one of the two possible product dissociation pathways is shown for clarity (P1 release prior to P2 release): reaction profile with saturating substrate at 1 M standard state and [E] ≪ 1 M (solid line) and reaction profile with subsaturating substrate at 1 fM standard state and [E] ≪ 1 fM (dotted line). The profile is drawn to scale, and the numbers refer to the actual free energy differences in kilocalories per mole. Equilibrium and rate constants were converted to $\Delta G°$ values using the equations $\Delta G° = -RT \ln K$ and $\Delta G^{\ddagger} = -RT \ln(hk/k_B T)$, respectively, in which R is the gas constant, T is the temperature in degrees kelvin (25 °C = 298 K), h is Planck's constant, and k_B is the Boltzmann constant.

type of kinetic or thermodynamic determination. The remaining rate constant, that for dissociation of S from the E·S complex, can be calculated from the measured values and the overall reaction equilibrium, as described below. Thus, the descriptions in Figure 10 and Figure 11 provide a kinetic and thermodynamic framework for a hammerhead ribozyme reaction in both the cleavage and ligation directions. The framework provides new insights into the behavior of the hammerhead ribozyme as a catalyst and as a structured RNA molecule.

Calculation of the Rate of Substrate Dissociation, k_{-1}. The pulse-chase experiments described above only provide an upper limit of $k_{-1} \leq 0.003$ min^{-1}. The value of k_{-1} can, however, be calculated from the overall or external equilibrium constant and the individual rate constants we have measured. The external equilibrium constant, $K_{eq}^{ext} = [P1][P2]/[S]$, describes the equilibrium concentrations of the substrate and products free in solution. This can be expressed as the ratio of all elemental rate constants of the ribozyme reaction, $K_{eq}^{ext} = k_1k_2k_3k_4/k_{-1}k_{-2}k_{-3}k_{-4}$. As all of the rate constants except k_{-1} have been measured, k_{-1} can be calculated if the value of K_{eq}^{ext} is known. The value has not been measured for the ribozyme substrates and products, but it can be estimated from a chemically identical cleavage reaction of the dinucleotide GpU to form guanosine 2′,3′-cyclic phosphate and uridine. A value of $K_{eq}^{ext} = 0.6$ M for this reaction was determined at 0 °C, pH 7.0, using RNase T1 to facilitate equilibration (Mohr & Thach, 1969). If water and uridine are assumed to behave similarly as nucleophiles in the opening of a 2′,3′-cyclic phosphate bond, K_{eq}^{ext} can be corrected to 25 °C using the enthalpy change for guanosine 2′,3′-cyclic phosphate hydrolysis, $\Delta H = -9.5$ kcal/mol (Rudolph et al., 1971). This small correction gives $K_{eq}^{ext} = 1.6$ M, which we use as an estimate for the external equilibrium constant for the HH16 reaction. Through some deviation for this calculation is anticipated due to the sequence differences and molecular structure of the oligonucleotides, these values are expected to represent reasonable estimates. With the measured elemental rate constants and the value of $K_{eq}^{ext} = 1.6$ M, the extremely low value of $k_{-1} = 1.5 \times 10^{-10}$ min^{-1} ($t_{1/2} \sim 9000$ years)[3] and a very low dissociation constant for the ribozyme/substrate complex of $K_d = k_{-1}/k_1 = 8 \times 10^{-18}$ M can be calculated.

Kinetic and Thermodynamic Reaction Profile. The results summarized in Figure 10 can be illustrated in the form of a free energy reaction profile (Figure 11). For the purpose of comparison, the reaction profile of the ribozyme-catalyzed reaction is illustrated at a 1 M standard state (solid line) and at a 1 fM standard state (dotted line), representing saturating and subsaturating conditions, respectively. For the standard state of 1 M, binding of S to E proceeds rapidly, and all substrate is initially trapped into an extremely stable E·S complex. Cleavage is strongly favored over substrate dissociation and ligation, ensuring efficient conversion of E·S to E·P1·P2. Free ribozyme is regenerated through the stepwise and rate-limiting process of product release. At the standard state of 1 M product (as depicted in Figure 11), it is energetically unfavorable to release the products due to strong product inhibition. Therefore, almost all ribozyme will be tied up in the E·P1·P2 complex. In the absence of free products, the standard assay conditions, the release of products from the ribozyme is rate-limiting and is an energetically "downhill" process. In contrast to the 1 M standard state, at the 1 fM standard state, binding of S to E is rate-limiting. Like in the 1 M standard state, upon E·S formation every substrate is committed to cleavage and subsequent product release due to the extremely slow substrate dissociation rate. Unlike the 1 M standard state, the reaction at 1 fM is an energetically "downhill" process, regardless of the presence or absence of 1 fM products, as there is no product inhibition at these concentrations. As shown in Figure 11, the external equilibrium K_{eq}^{ext} depends on the standard state chosen because two molecules are formed from one molecule in the solution reaction. For example, at the standard state of 1 M concentrations, approximately equal amounts of substrate and products exist in solution at equilibrium while at 1 fM only 1 in approximately 10^{15} molecules exist as S. On the other hand, the internal states of the ribozyme-catalyzed reaction reflect an intramolecular process, and are therefore independent of the solution concentrations. K_{eq}^{int} is 130.

Internal Equilibrium Constant. The rate of ligation is slower than the rate of cleavage, giving an internal equilibrium constant of about 130. Thus, the formation of products is favored on the ribozyme. What structural and mechanistic implications can be drawn from the result? At the level of bond energies, product formation would not be favored, since there is evidence for strain within a pentacyclic phosphate ring, suggesting that the intrinsic bond energy of a 2′,3′-cyclic diester bond (N>p) is greater than that of a 3′–5′ linkage (NpN) (Kumamoto et al., 1956; Gerlt et al., 1975). The fact that the ribozyme drives the equilibrium toward product formation suggests that a favorable entropic contribution outweighs the unfavorable generation of a 2′,3′-cyclic diester bond. This suggests that E·S can be envisioned as a complex having restricted internal motion with respect to E·P1·P2. Upon cleavage of S, the acquired motion introduces a "floppiness" to the complex E·P1·P2, providing an entropic advantage for the formation of products on the ribozyme. Alternatively, the internal equilibrium could be driven toward product formation if the ribozyme can form specific inter-

[2] $k_{cat} = [E_t]/(1/k_2' + 1/k_{3,5}')$; $k_2' = k_2(k_3 + k_5)/(k_{-2} + k_3 + k_5)$; $k_{3,5}' = (k_3 + k_5)/(1 + k_3/k_4 + k_5/k_6)$. The rate constants are defined in Figure 2; k_2' and $k_{3,5}'$ are the net rate constants for the cleavage step and the product release step, respectively.

[3] Direct measurement of the rate constant of substrate dissociation for HH16 or the external equilibrium constant using HH16 to catalyze equilibration is precluded by this extremely slow rate constant.

actions with the products and not with the substrate. However, as discussed below, neither product binds to the ribozyme more strongly than expected from a simple duplex, providing no indication of such favorable interactions.

The implied floppiness of the ribozyme/product complex can be described formally in terms of the "effective concentration" (EC). EC describes the ability to form S from from P1 and P2 on the ribozyme relative to the equilibrium for S formation in solution (K_{eq}^{int} = [E·P1·P2]/[E·S]; K_{eq}^{ex} = [P1]·[P2]/[S]; EC = K_{eq}^{ex}/K_{eq}^{int}). Because the reaction is intramolecular on the ribozyme but intermolecular in solution, the EC has units of molar. For the hammerhead ribozyme reaction, the EC = K_{eq}^{ex}/K_{eq}^{int} = 10^{-2} M. This may provide a description of how precisely the ribozyme positions P1 and P2 for reaction. P1 and P2 behave on the ribozyme as if they were present in solution at a concentration of 10^{-2} M. Thus, binding to the ribozyme provides an entropic advantage for ligation at concentrations $<10^{-2}$ M. However, with P1 and P2 more concentrated than 10^{-2} M, the extent of ligation would be greater free in solution than on the ribozyme. This is depicted in Figure 11. For the standard state of 1 fM, the formation of S from P1 and P2 is more favorable on the ribozyme than in solution, but for the standard state of 1 M, the formation of S is more favorable in solution than in the E·P1·P2 complex.

While the hairpin ribozyme catalyzes the same phosphodiester cleavage reaction as the hammerhead (Buzayan et al., 1986a), it is better than the hammerhead at ligation. The internal equilibrium has been measured to be approximately 1 (Buzayan et al., 1986a; Chowrira et al., 1993; Feldstein & Bruening, 1993). Therefore, the effective concentration of the hairpin ribozyme is about 1 M, or about 100-fold higher than that for the hammerhead ribozyme. This suggests that the hairpin ribozyme is better in orienting products for ligation than the hammerhead ribozyme by approximately 3 kcal/mol. This difference could be the result of a more rigid structure of the hairpin than of the hammerhead ribozyme.

The EC's of 0.01–1 M observed in the hammerhead and hairpin ribozyme reactions are quite small compared to EC's of 10^4–10^5 M observed with several protein enzymes (Thompson, 1974; Bode, 1979; Nakamura & Abeles, 1985). The theoretical maximum EC of 10^8 M, representing the loss of entropy in forming a covalent bond to join two molecules, is even larger (Page & Jencks, 1975). Thus, it appears that neither ribozyme is as good in precise positioning as are several protein enzymes. It remains to be determined whether larger RNA enzymes are better at aligning reactants.

The measurement of the internal equilibrium constant, K_{eq}^{int}, and the resultant determination of the EC provide a crude structural picture of the ribozyme. The ability to measure the reaction in both directions will now allow determination of the effect of reaction conditions and mutations both on the rate of cleavage and on the value of K_{eq}^{int}. It will be of considerable interest to determine whether there are ribozyme residues or functional groups for which "catalytic" and "structural" contributions can be differentiated.

Biological Implications of the Reverse Reaction and the Internal Equilibrium. In its biological context, the hammerhead is embedded within the genomic sequence of much larger RNAs. For example, the hammerhead is found at the ends of the linear satellite RNA of tobacco ringspot virus (Prody et al., 1986), as a contiguous sequence within the genomes of several circular virusoid RNA genomes (Forster & Symons, 1987a), or as two noncontiguous portions of the avocado sunblotch viroid RNA genome (Hutchins et al., 1986). In each case, the self-cleavage activity is believed to be responsible for the processing of the multimeric genomes that arise during replication. Since the rolling-circle replication mechanism also requires ligation of monomeric genomes into circles (Branch & Robertson, 1984), it has been proposed that this circularization step may be the autocatalytic reversal of the cleavage reaction (Forster & Symons, 1987a).

Our observation that the internal equilibrium is quite far in the direction of cleavage is consistent with the observation that quite low concentrations of multimeric genomes are generally found in infected plant cells (Keese & Symons, 1987). In addition, our data are consistent with the relatively efficient *in vitro* cleavage of dimers of STobRV(+) and the inefficient ligation of STobRV(+) monomers into dimers (Prody et al., 1986). However, in apparent contrast to these results, there are a considerable number of RNAs which contain hammerheads but are in a circular form within cells and even remain circular when isolated biochemically (Keese & Symons, 1987). Several lines of evidence suggest that these RNAs are folded into conformations that do not permit the hammerhead to form and therefore they do not reflect the internal equilibrium of the hammerhead. Heating and cooling circular vLTSV RNA appear to rearrange a fraction of the molecules into a conformation that will cleave (Forster & Symons, 1987a). Deleting RNA sequences that stabilize nonhammerhead conformations in vLTSV also improves the cleavage extent *in vitro* (Forster & Symons, 1987b). Finally, mutants of STobRV RNA in nonhammerhead sequences increase the accumulation of multimeric forms, suggesting the formation of new alternative structures that cleave less efficiently (Robaglia et al., 1993). Thus, an internal equilibrium that greatly favors cleavage is not at odds with any biological data.

It is possible that the 0.5–1% ligation predicted by the internal equilibrium can provide enough circular RNAs to permit efficient replication. Alternatively, the fraction of circular RNA may be much greater if, after the ligation event, hammerhead-containing RNAs readily adopt stable conformations that do not cleave. Perhaps cellular proteins favor the rearrangement by preferentially binding the small fraction of circles. Alternatively, the known plant RNA ligase can covalently join the hammerhead termini and simultaneously introduce a 2′-phosphate that will block self-cleavage (Kikuchi et al., 1982). The presence of the 2′-phosphate group at the cleavage site or removal of the 2′-phosphate after a conformational rearrangement step would ensure an increased concentration of circular RNAs. The existence of a 2′-phosphate at the hammerhead cleavage site in some, but not all, virusoids supports such an RNA ligase mechanism (Kiberstis et al., 1985).

Interaction of the Ribozyme with Its Cleavage Products. Both products bind tightly to HH16 after cleavage. The rate constants for product association are between 5×10^7 and 10^8 M^{-1} min^{-1}. These rate constants are approximately 10^3–10^4-fold slower than the rate of diffusional encounter, 10^{11} M^{-1} min^{-1} (Eigen & Hammes, 1963), but similar to values for helix formation between oligonucleotides (Craig et al., 1971; Pörschke & Eigen, 1971; Pörschke et al., 1973; Ravetch et al., 1974; Breslauer & BinaStein, 1977; Breslauer et al., 1982; Nelson & Tinoco, 1982). Oligonucleotide association rates of other hammerheads and the *Tetrahymena* group I ribozyme have also been found to be in the range of 10^7–10^8 M^{-1} min^{-1} (Herschlag & Cech, 1990; Bevilacqua et al., 1992; Fedor & Uhlenbeck, 1992). On the basis of these comparisons, the observed product association rate constants are within the range of expected values. This suggests that the assembly of

ribozyme/product complexes is dominated by simple helix formation.

In order to determine if the product affinities measured correspond to thermodynamic predictions for simple duplexes in the absence of conserved ribozyme core nucleotides, the stabilities of E·P1 and E·P2 complexes were calculated on the basis of nearest-neighbor contributions at 25 °C (Freier et al., 1986). The value of $\Delta G°$ = −13.0 kcal/mol measured for the E·P2 complex is in excellent agreement with the calculated value of $\Delta G°$ = −13.6 kcal/mol. A similar close agreement between the measured and the predicted $\Delta G°$ for P2 was observed with a different hammerhead (Fedor & Uhlenbeck, 1992). A value for E·P1 affinity was measured here for the first time to be $\Delta G°$ = −12.1 kcal/mol. This is a 2.2 kcal/mol lower affinity than the value of $\Delta G°$ = −14.3 kcal/mol calculated from nearest-neighbor values. It is currently unclear if this difference reflects the different salt conditions used in obtaining the nearest-neighbor values (1 M NaCl) or effects imposed by the ribozyme structure. Nevertheless, it appears that unlike the *Tetrahymena* group I ribozyme which binds its product 10^4-fold tighter than expected from base-pairing interactions alone (Herschlag & Cech, 1990; Pyle et al., 1990; Bevilacqua & Turner, 1991), the products of the hammerhead ribozyme motif do not bind considerably stronger then expected from simple helices. P1 may bind somewhat weaker. This is currently under investigation.

The kinetic and binding data indicate that the product binding affinity is increased 0.8–1 kcal/mol (4–5-fold) in the presence of the other product. This effect is comparable in magnitude to RNA helix stabilization gained through 3′ dangling nucleotides or even an additional base pair (Freier et al., 1986). As expected from the thermodynamic cycle, the presence of P1 increases the affinity of P2 to the same extent as the presence of P2 increases that of P1. The modest stabilization is accounted for by a 2-fold increase in the association rate constant and a 2-fold decrease in the dissociation rate constant of each product. Considering the "floppiness" of the E·P1·P2 complex as argued above, it seems unlikely that stacking interactions between P1 and P2 could lend to the 2-fold decrease in the dissociation rate constant. Models that could account for the increased affinities include the formation of an additional metal binding pocket, magnesium coating of the RNA duplex, or disruption of intramolecular structure within the ribozyme upon binding of the first product oligonucleotide.

Interaction of the Ribozyme with Its Substrate. The rate constant of substrate association is 2×10^7 M^{-1} min^{-1}. As argued above for the products, such an association rate constant is within the range of expected values for RNA helices so that the assembly of E·S is presumably also dominated by the process of simple helix formation. The 3–5-fold slower association rate constant of S compared to the products may originate from alternate conformations of S that hinder its binding to the ribozyme.

The rate of substrate dissociation, k_{-1}, was calculated to be about $k_{-1} \sim 1.5 \times 10^{-10}$ min^{-1}. A comparison of this extremely slow dissociation rate constant with the cleavage rate constant suggests that essentially every substrate that binds the ribozyme will be processed to products. Analogous behavior has been observed for the *Tetrahymena* group I ribozyme (Herschlag & Cech, 1990). The slow substrate dissociation rate constant also suggests that HH16 is expected to bind efficiently to oligonucleotides containing one or more mismatches within helices I and III. As a consequence, the mismatched oligonucleotides would be efficiently recognized as substrates and cleaved to products. Experiments addressing substrate specificity are currently in progress. In general, it may be easy to create a ribozyme that favors cleavage of a substrate over its dissociation by simply lengthening regions of base-pairing. The tradeoff for ribozymes as multiple turnover catalysts that apparently arises is that longer recognition sequences slow product release, lowering the value of k_{cat} and allowing the ribozyme to be saturated at lower concentrations of substrate.

The value of ΔG^{ES} = −23.6 kcal/mol was estimated from the external equilibrium and all other elemental rate constants. If helices I and III are assumed not to stack on each other, the nearest-neighbor contributions (Freier et al., 1986) give a total $\Delta G°$ of −30.3 kcal/mol at 25 °C ($\Delta G° = \Delta G^{\text{helix I}} + \Delta G^{\text{helix II}} + \Delta G^{\text{initiation}}$). The difference in stability between predicted and observed values, $\Delta\Delta G$ = 6.7 kcal/mol, might then reflect the destabilizing thermodynamic contribution of the "single-stranded" core nucleotides. This value is similar to the destabilization of a complementary RNA helix containing a bulge loop of three nucleotides ($\Delta G° \sim$ 6.4 kcal/mol) (Longfellow et al., 1990) or an extremely asymmetric internal loop with six unpaired A nucleotides ($\Delta G°$ = 4.6 kcal/mol) (Peritz et al., 1991). We have performed the same calculation for a different hammerhead (HH8) for which ΔG^{ES} was measured to be −10 kcal/mol (Fedor & Uhlenbeck, 1992). A quite similar value of $\Delta\Delta G$ = 5 kcal/mol was obtained, suggesting that the hammerhead core nucleotides might have a uniform thermodynamic contribution. However, when this calculation was done for a third hammerhead (HH13; Fedor & Uhlenbeck, 1992), a significantly different value of $\Delta\Delta G$ = 10 kcal/mol was obtained. We are currently reinvestigating the HH13 reaction and several other hammerheads in order to understand this apparent discrepancy. If the trend of a fixed destabilizing core contribution is solidified by analysis of other hammerhead systems, all pre-steady-state and steady-state rate constants for a given hammerhead should be predictable from this value of the constant $\Delta\Delta G$, the known thermodynamic parameters for helix formation (Freier et al., 1986), and the rate constants determined herein.

ACKNOWLEDGMENT

We thank Dave Long, Tracy Stage, Tao Pan, and Tim McConnell for critical reading of the manuscript.

REFERENCES

Branch, A. D., & Robertson, H. D. (1984) *Science 223*, 450–455.

Bevilacqua, P. C., & Turner, D. H. (1991) *Biochemistry 30*, 10632–10640.

Bevilacqua, P. C., Kierzeck, R., Johnson, K. A., & Turner, D. H. (1992) *Science 258*, 1355–1358.

Bode, W. (1979) *J. Mol. Biol. 127*, 357–374.

Breslauer, K. J., & Bina-Stein, M. (1977) *Biophys. Chem. 71*, 211–216.

Breslauer, K. J., Frank, R., Bloecker, H., & Marky, L. A. (1986) *Proc. Natl. Acad. Sci. U.S.A. 83*, 3746–3750.

Buzayan, J. M., Gerlach, W. L., & Breuning, G. (1986a) *Nature 323*, 349–353.

Buzayan, J. M., Gerlach, W. L., & Breuning, G. (1986b) *Proc. Natl. Acad. Sci. U.S.A. 83*, 8859–8862.

Chowrira, B. M., Berzal-Herranz, A., & Burke, J. M. (1993) *Biochemistry 32*, 1088–1095.

Cleland, W. W. (1975) *Biochemistry 14*, 3220–3224.

Craig, M. E., Crothers, D. M., & Doty, P. (1971) *J. Mol. Biol. 62*, 383–401.

Dahm, S. C., & Uhlenbeck, O. C. (1991) *Biochemistry 30*, 9464–9469.

Dahm, S. C., Derrick, W. B., & Uhlenbeck, O. C. (1993) *Biochemistry 32*, 13040–13045.
Eigen, M., & Hammes, G. G. (1963) *Adv. Enzymol. Relat. Areas Mol. Biol. 25*, 1–38.
England, T. E., & Uhlenbeck, O. C. (1978) *Biochemistry 17*, 2069–2076.
Fedor, M. J., & Uhlenbeck, O. C. (1990) *Proc. Natl. Acad. Sci. U.S.A. 87*, 1668–1672.
Fedor, M. J., & Uhlenbeck, O. C. (1992) *Biochemistry 31*, 12042–12054.
Feldstein, P. A., & Bruening, G. (1993) *Nucleic Acids Res. 21*, 1991–1998.
Fierke, C. A., Johnson, K. A., & Benkovic, S. J. (1987) *Biochemistry 26*, 4085–4092.
Forster, A. C., & Symons, R. H. (1987a) *Cell 49*, 211–220.
Forster, A. C., & Symons, R. H. (1987b) *Cell 50*, 9–16.
Freier, S. M., Kierzek, R., Jaeger, J. A., Sugimoto, N., Caruthers, M. H., Neilson, T., & Turner, D. H. (1986) *Proc. Natl. Acad. Sci. U.S.A. 83*, 9373–9377.
Gerlt, J. A., Westheimer, F. H., & Sturtevant, J. M. (1975) *J. Biol. Chem. 250*, 5059–5067.
Haseloff, J., & Gerlach, W. L. (1988) *Nature 334*, 585–591.
Hertel, K. J., Pardi, A., Uhlenbeck, O. C., Koizumi, M., Ohtsuka, E., Uesugi, S., Cedergren, R., Eckstein, F., Gerlach, W., Hodgson, R., & Symons, R. H. (1992) *Nucleic Acids Res. 20*, 3252.
Herschlag, D., & Cech, T. R. (1990) *Biochemistry 29*, 10159–10171.
Hutchins, C. J., Rathjen, P. D., Forster, A. C., & Symons, R. H. (1986) *Nucleic Acids Res. 14*, 3627–3640.
Jencks, W. P. (1975) *Adv. Enzymol. Relat. Areas Mol. Biol. 43*, 219–410.
Jeffries, A. C., & Symons, R. H. (1989) *Nucleic Acids Res. 17*, 1371–1377.
Keese, P., & Symons, R. H. (1987) in *Viroids and Viroid-like Pathogens* (Semancik, J. S., Ed.) pp 1–47, CRC Press, Boca Raton, FL.
Kiberstis, P. A., Haseloff, J., & Zimmern, D. (1985) *EMBO J. 4*, 817–822.
Kikuchi, Y., Tyc, K., Filipowicz, W., Sänger, H. L., & Gross, H. J. (1982) *Nucleic Acids Res. 10*, 7521–7529.
Kochino, Y., Watanabe, S., Harada, F., & Nishimura, S. (1980) *Biochemistry 19*, 2085–2089.
Koizumi, M., Iwai, S., & Ohtsuka, E. (1988) *FEBS Lett. 228*, 228–230.
Koizumi, M., Hayase, Y., Iwai, S., Kamiya, H., Inoue, H., & Ohtsuka, E. (1989) *Nucleic Acids Res. 17*, 7059–7071.
Kumamoto, J., Cox, J. R., & Westheimer, F. H. (1956) *J. Am. Chem. Soc. 78*, 4858–4860.
Longfellow, C. E., Kierzek, R., & Turner, D. H. (1990) *Biochemistry 29*, 278–285.
Milligan, J. F., & Uhlenbeck, O. C. (1989) *Methods Enzymol. 180*, 51–62.
Mohr, S. C., & Thach, R. E. (1969) *J. Biol. Chem. 244*, 6566–6576.
Nakamura, C. E., & Abeles, R. H. (1985) *Biochemistry 24*, 1364–1376.
Naylor, R., & Gilham, P. T. (1966) *Biochemistry 5*, 2722–2726.
Nelson, J. W., & Tinoco, I., Jr. (1982) *Biochemistry 21*, 5289–5295.
Page, M. I., & Jencks, W. P. (1971) *Proc. Natl. Acad. Sci. U.S.A. 68*, 1678–1683.
Peritz, A. E., Kierzek, R., Sugimoto, N., & Turner, D. H. (1991) *Biochemistry 30*, 6428–6436.
Perreault, J.-P., Labuda, D., Usman, N., Yang, J.-H., & Cedergren, R. (1991) *Biochemistry 30*, 4020–4025.
Pieken, W. A., Olsen, D. B., Benseler, F., Aurup, H., & Eckstein, F. (1991) *Science 253*, 314–317.
Pörschke, D., & Eigen, M. (1971) *J. Mol. Biol. 62*, 361–381.
Pörschke, D., Uhlenbeck, O. C., & Martin, F. H. (1973) *Biopolymers 12*, 1313–1335.
Prody, G. A., Bakos, J. T., Buzayan, J. M., Schneider, I. R., & Bruening, G. (1986) *Science 231*, 1577–1580.
Pyle, A. M., McSwiggen, J. A., & Cech, T. R. (1990) *Proc. Natl. Acad. Sci. U.S.A. 87*, 8187–8191.
Ravetch, J., Gralla, J., & Crothers, D. M. (1974) *Nucleic Acids Res. 1*, 109–127.
Robaglia, C., Bruening, G., Haseloff, J., & Gerlach, W. L. (1993) *EMBO J. 12*, 2969–2976.
Rudolph, S. A., Johnson, E. M., & Greengard, P. (1971) *J. Biol. Chem. 246*, 1271–1273.
Ruffner, D., Dahm, S. C., & Uhlenbeck, O. C. (1989) *Gene 82*, 31–41.
Sampson, J. R., Sullivan, F. X., Behlen, L. S., DiRenzo, A. B., & Uhlenbeck, O. C. (1987) *Cold Spring Harbor Symp. Quant. Biol. 51*, 4330–4335.
Thompson, R. C. (1974) *Biochemistry 13*, 5495–5501.
Uhlenbeck, O. C. (1987) *Nature 328*, 596–600.
Uhlenbeck, O. C. (1993) in *Antisense Research and Application* (Crooke, S. T., & Lebleu, B., Eds.) pp 83–96, CRC Press, Boca Raton, FL.
Woodson, S. A., & Cech, T. R. (1989) *Cell 57*, 335–345.